V European Conference on Computational Fluid Dynamics
ECCOMAS CFD 2010
J. C. F. Pereira and A. Sequeira (Eds)
Lisbon, Portugal, 14–17 June 2010

MULTI-STAGE DESIGN APPROACH FOR HIGH FIDELITY AERODYNAMIC OPTIMIZAITON OF MULTI-BODY GEOMETRIES BY KRIGING BASED MODEL AND ADJOINT VARIABLE METHOD

JinWoo Yim[*], ByungJoon Lee[†] and Chongam Kim[††]

[*]School of Mechanical & Aerospace Eng., Seoul National Univ.
599 Gwanak-ro, Gwanak-gu, Seoul, 151-742, Korea
baccha@freechal.com

[†]NASA Glenn Research center
21000 Brookpark Road, Cleveland, OH, 44135, USA
mecha777@hitel.net

[††]School of Mechanical & Aerospace Eng., Seoul National Univ.
599 Gwanak-ro, Gwanak-gu, Seoul, 151-742, Korea
chongam@snu.ac.kr (Corresponding Author)

Key words: Aerodynamic Shape optimization, GA, Kriging, Adjoint Variable Method

Abstract. *An efficient and high-fidelity design approach for wing-body configuration is presented. Depending on the size of design space and the number of design of variable, aerodynamic shape optimization is carried out via selective optimization strategy at each design stage. In the first stage, global optimization techniques are applied to planform design with a few geometric design variables. In the second stage, local optimization techniques are employed for wing surface design with a lot of design variables which can maintain a sufficient design space with a high DOF (Degree of Freedom) geometric change. For global optimization, Kriging method in conjunction with GA (Genetic Algorithm) is used. A searching algorithm of EI (Expected Improvement) points is introduced to enhance the quality of global optimization for the wing-planform design. For local optimization, a discrete adjoint method is adopted, and adjoint numerical dissipation is introduced to improve convergence behavior of the adjoint solver. By the successive combination of global and local optimization techniques, drag minimization is performed for a multi-body aircraft configuration in inviscid and viscous flow conditions while maintaining the baseline lift and the wing weight. Through the design process, performances of the test models are remarkably improved in comparison with the single stage design approach. The performance of the proposed design framework including wing planform design variables can be efficiently evaluated by the drag decomposition method, which can examine the improvement of various drag components, such as induced drag, wave drag and viscous drag.*

1 INTRODUCTION

Aerodynamic shape optimization using numerical methods becomes more and more popular in the area of aircraft design along with growth of computational power. The progress of computing environment also makes the choice of optimization methods more flexible than before. Nevertheless, it is still recommended that a design strategy has to be judiciously chosen by considering the characteristics of design problems. For example, highly non-linear characteristics of design space prohibit designers from selecting gradient-based optimization method since the gradient-based method can lead to a designed geometry trapped in a local optimum. The design methodologies can be roughly classified into gradient and non-gradient methods depending on the usage of sensitivity analysis process. Non-gradient optimization methods can be usually called global optimization method, while gradient-based method can be classified into local optimization method.

Global optimization method may provide the global optimum value within the specified design space. For example, Genetic Algorithm (GA) originated from the theory of natural evolution is widely used as a global optimization tool[1,2,3]. However, this method is generally costly in imitating an accurate evolutional process, and especially for three-dimensional aerodynamic design problems with a lot of design variables, it requires an enormous amount of computational time in evaluating experimental data at each deign point. For that reason, GA as an aerodynamic shape optimization is generally applied to problems with a relatively small number of design variables. Therefore, approximation technique, called meta-modeling originated from statistics, is popularly adopted, such as RSM (Response Surface Method)[4,5] or Kriging[6,7]. Once a meta-modeling is constructed by a suitable mathematical function and experimental data points in design space, it can predict new values without additional flow analysis. However, these modeling methods may also require a huge computational cost to obtain sufficient experimental data for building up the response model, if geometric shape is complex or the number of design variable is large. Furthermore, if sample experimental points representing objective function values are not appropriate, design results can be poorer than other optimization tools. As an improved meta-modeling, optimization based on Kriging model is applied for the robust exploration of the global optimum value. Jones *et al.*[8] firstly introduced the Expected Improvement (EI) method proposed by Mockus *et al.*[9] into Kriging model, and Jeong *et al.*[10] applied it to shape optimization.

On the other hand, Gradient-Based Optimization Method (GBOM) is also popularly used because computational cost of adjoint approach is essentially independent of the number of design variable. In addition, it exhibits a good convergence characteristic because GBOM uses the gradient vector of the objective function which provides an optimal direction in design space. Thus, it is particularly powerful in case of wing surface design which usually requires a lot of design variables. Jameson *et al.*[11] proposed continuous adjoint approach, and applied it to aerodynamic shape optimization problems of several wing/body geometries with wing planform and surface design variables. Lee *et al.*[12,13] extended the discrete adjoint method to overset mesh system, which can be applied to complex geometries with a relatively simple grid topology. Mavriplis[14], Nielsen[15] and Kim[16] *et al.* also used the discrete adjoint method in design problems of various complex geometries on unstructured mesh system. Through these applications, continuous or discrete adjoint variable methods have been demonstrated the capability to produce a substantial improvement of aerodynamic performance. Despite the superior performance in aerodynamic design problems,

GBOM still has a potential danger to be trapped in local optimum during design process, especially in cases of noisy non-linear design spaces.

In the present study, an efficient multi-stage design strategy is proposed which takes advantages of both global and local optimization methods. Transonic wing and DLR-F4 wing body configuration is re-designed using proposed design strategy in inviscid and viscous flow conditions. Wing planform design which can be represented with a few design variables is performed by global optimization method using an improved Kriging method and GA optimizer. On the other hand, wing surface design which requires a lot of design variables for the sophisticated treatment of surface geometry is performed by GBOM using the discrete adjoint approach. To improve the convergence in sensitivity analysis, numerical dissipation for the discrete adjoint formulation proposed by Lee *et al*.[17,18] is introduced. Finally, capability of the proposed multi-stage design approach including wing planform design variables is evaluated by drag decomposition method based on far-field analysis[19,20,21,22], which can provide behavior of each drag component before and after design process.

2 NUMERICAL METHODS

2.1 Kriging Method

Meta-modeling techniques are commonly used to create approximation of the mean and variation of response in noisy design space, because their implementation is relatively simple. A meta-model is adopted as a surrogate approximation for actual experimental data or numerical analysis during design process. Among the meta-modeling techniques, RSM and Kriging model are most popular techniques in aerodynamic shape design. RSM employs a simple polynomial function using the least square regression technique. For that reason, RSM has a limitation if physical phenomena are highly non-linear or noisy with respect to design variables. On the other hand, Kriging method is more flexible in dealing with aerodynamic design problems of highly non-linear design space[6,7,8,9,10]. Kriging method was developed in the field of geostatistics, and it is useful in predicting temporally and spatially correlated data. A most distinguished advantage of Kriging model is that it can exactly interpolate sample data, and represent a function with multiple local extrema. As in Eqn. (1), Kriging modeling technique is composed of two elements.

$$y(x) = \beta + Z(x) \tag{1}$$

where β is a global regression model such as RSM or usually a constant value. x is an n-dimensional design vector where n is the number of design variable. $Z(x)$ is the realization of stationary Gaussian random function to calibrate local deviation from the global model. Multiple local extrema can be represented by this term, and thus, Kriging method may be more suitable than RSM in fitting design space if physical phenomena are highly non-linear or noisy. The covariance matrix of $Z(x)$ is given by

$$Cov\left[Z\left(x^i\right), Z\left(x^j\right)\right] = \sigma^2 \mathbf{R}\left[R\left(x^i, x^j\right)\right] \tag{2}$$

where $\mathbf{R}$ is the correlation matrix, and $R(x^i, x^j)$ is a correlation function between any two sample data points, x^i and x^j. In the present work, the Gaussian correlation function is used as follows.

$$R\left(x^i, x^j\right) = \exp\left[-\sum_{k=1}^{n_{DV}} \theta_k \left|x_k^i - x_k^j\right|^2\right] \tag{3}$$

In Eqn. (3), θ_k are unknown correlation parameters to fit the model, and $\left|x_k^i - x_k^j\right|$ is the distance between the k^{th} component of the sample points x^i and x^j. Once the correlation function is determined, predicted estimate, $\hat{y}(x)$, for the response, $\mathbf{y}$, at untried value of x is given by Eqn. (4).

$$\hat{y}(x) = \hat{\beta} + \hat{\mathbf{r}}^{\mathbf{T}}(x)\mathbf{R}^{-1}(\mathbf{y} - \mathbf{f}\hat{\beta}) \tag{4}$$

where $\hat{\beta}$ is the estimated value of β, and $\mathbf{y}$ is a column vector of length n_s (the number of sample point) that contains the response values at each sample point. $\hat{\mathbf{r}}^{\mathbf{T}}(x)$ is the correlation vector of length n_s between an untried x and the sample points, and it is defined as follows.

$$\mathbf{r}^{\mathbf{T}}(x) = \left[R(x, x^1), R(x, x^2), ..., R(x, x^{n_s}),\right]^T \tag{5}$$

For any given correlation parameters θ, $\hat{\beta}$ and the estimated variance $\hat{\sigma}^2$ are determined as

$$\hat{\beta} = (\mathbf{f}^{\mathbf{T}}\mathbf{R}^{-1}\mathbf{f})^{-1}\mathbf{f}^{\mathbf{T}}\mathbf{R}^{-1}\mathbf{y} \tag{6}$$

$$\hat{\sigma}^2 = \frac{(\mathbf{y} - \mathbf{f}\hat{\beta})^T \mathbf{R}^{-1}(\mathbf{y} - \mathbf{f}\hat{\beta})}{n_s} \tag{7}$$

where $\mathbf{f}$ is a vector of ones with n_s -dimensional length. Finally, the correlation parameter θ_k is estimated by maximizing the likelihood function (Eqn. (8)) over $\theta_k > 0$, and Genetic Algorithm (GA) is used to find the θ_k in this work.

$$Ln(\theta) = -\frac{\left[n_s \ln(\hat{\sigma}^2) + \ln|\mathbf{R}|\right]}{2} \tag{8}$$

Thus, the distance function between sample points, as in Eqn. (3), is not equally weighted. Once θ_k is determined, $\hat{\sigma}^2$ and $|\mathbf{R}|$ can be calculated by the correlation parameters. Finally, the predicted values at untried x are obtained from Eqn. (4).

The accuracy of Kriging method between predicted and real values is seriously affected by sample data points. If the number of sample point is not sufficient and/or inappropriate sample points are selected, the predicted response surface yields inaccurate information which eventually leads to unsatisfactory design result. The accuracy of the predicted values at untried x can be expressed as

$$s^2(x) = \hat{\sigma}^2\left[1 - \mathbf{r}^{\mathbf{T}}\mathbf{R}^{-1}\mathbf{r} + \frac{(1 - \mathbf{f}^{\mathbf{T}}\mathbf{R}^{-1}\mathbf{r})^2}{\mathbf{f}^{\mathbf{T}}\mathbf{R}^{-1}\mathbf{f}}\right] \tag{9}$$

where $s^2(x)$ is the mean square error of the predictor, and it represents some uncertainty at the predicted point. The root mean square error can be expressed as $s = \sqrt{s^2(x)}$.

2.2 Expected Improvement

Once a Kriging model is constructed, GA is used to search the global optimum value within the specified design space. Thus, there is a possibility that the global optimum value given by GA may not be the global optimum in the real design space. As a way to find more accurate response surface and more efficient exploration for global optimum point, EI (Expected Improvement) has been proposed or applied[8,9,10].

The main idea is that the uncertainty of the predicted value should be taken into account in sampling additional point for the initial Kriging model. In this process, EI basically provides a kind of figure of merit (or a value of expected improvement) when additional sample point is added to existing sample data. For example, during the minimizing process of the objective function, EI can be formulated and expressed in a closed form as in Eqns. (10) and (11).

$$I(x) = \begin{cases} f_{\min} - \hat{y}(x), \; if \;\; \hat{y} < f_{\min} \\ 0 \qquad\qquad\quad ,otherwise \end{cases} = \max\left[f_{\min} - \hat{y}(x), 0\right] \tag{10}$$

$$E\left[I(x)\right] = (f_{\min} - \hat{y})\Phi\left(\frac{f_{\min} - \hat{y}}{s}\right) + s\phi\left(\frac{f_{\min} - \hat{y}}{s}\right) \tag{11}$$

where $f_{\min}$ is the minimum value predicted by the initial Kriging model. Φ and ϕ are the normal distribution and normal density functions. From Eqn. (11), the maximum EI point can be evaluated, and the value of the sample point obtained by CFD solver is added. If the objective function value of the sample point is smaller than the current minimum value, $f_{\min}$ is newly updated. This process is iteratively performed and stopped until the EI becomes less than some threshold criterion. Through the Kriging-EI process, the point nearer the global optimum can be predicted in the specified design space. Figures 1 to 6 show the Kriging model with EI approach. At the initial step (Figure 2), response surface approximated by Kriging with initial sample points does not accurately fit the real surface. Based on EI points as shown Figures 3 to 5, additional sample points are predicted and added to sample data. After this step, improved response surface is obtained as shown Figure 6.

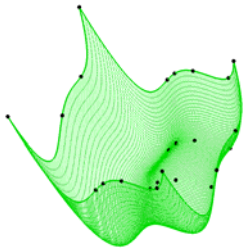

Figure 1: Real function & initial sample points

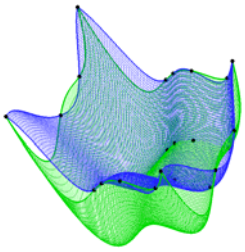

Figure 2: Kriging model with initial smaple points

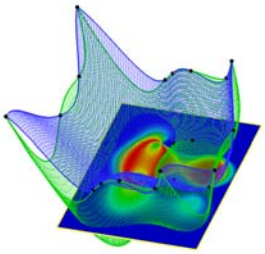

Figure 3: EI at initial step

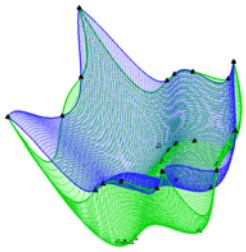

Figure 4: Additional sample points from EI

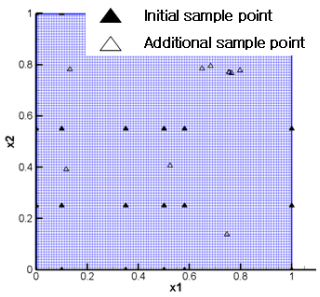

Figure 5: Additional sample points from EI

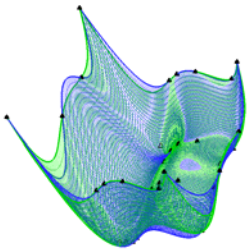

Figure 6: Final kriging model with EI points

2.3 Genetic Algorithm

Genetic Algorithm (GA) is a class of stochastic algorithm inspired by natural evolution, and has been applied to find optimum values in various fields. Starting with a

randomly generated population of chromosomes, a GA goes through a process of fitness based selection and recombination to produce successor population or the next generation. During recombination, parent chromosomes are selected and their genetic material is recombined to generate the child generation. As this process is progressed iteratively, a sequence of successive generations evolves and average fitness of the chromosomes tends to increase until stopping criterion is reached. In this way, a GA evolves into the best solution to a given design problem. An advantage of GA is that, unlike other optimization algorithms, it does not need gradient information. Therefore, if there are many local extrema and discontinuous properties in objective functions and constraints, GA is more suitable in finding the global optimization point and design variable set than gradient-based optimization methods. On the other hand, a GA requires substantial computational cost because of a large number of function evaluations. For that reason, it may be prohibitive to directly apply to complex aerodynamic shape optimization with a large number of design variables.

2.4 Discrete Adjoint Approach

If design space contains multiple local extrema and discontinuities, non-gradient optimization methods such as GA could be more suitable to find optimum values. On the other hand, if design space is relatively (or locally) smooth and continuous, gradient-based methods are much more efficient because of a good convergence behavior. Especially, adjoint variable method is the most powerful technique among the gradient-based methods, because computational cost to solve the adjoint equation is not essentially influenced by the number of design variable. This is particularly useful when there are a lot of design variables such as wing surface design.

In the present paper, discrete adjoint variable method is applied to get sensitivity information by fully hand differentiating the three-dimensional Euler and N-S equations. The symbolic formulation of the discrete residual R for the steady-state flow equations can be written as

$$\{R\} = \{R(Q, X, D)\} = \{0\} \tag{12}$$

where Q is the flow variable vector, X is the position of computational grid and D is the vector of design variables. Without evaluating the vector dQ/dD, the sensitivity derivative of the objective function, $F = F(Q,X,D)$, can be calculated as

$$\left\{\frac{dF}{dD}\right\} = \left\{\frac{\partial F}{\partial Q}\right\}^T \left\{\frac{dQ}{dD}\right\} + \left\{\frac{\partial F}{\partial X}\right\}^T \left\{\frac{dX}{dD}\right\} + \left\{\frac{\partial F}{\partial D}\right\} + \Lambda^T \left(\left[\frac{\partial R}{\partial Q}\right]\left\{\frac{dQ}{dD}\right\} + \left[\frac{\partial R}{\partial X}\right]\left\{\frac{dX}{dD}\right\} + \left\{\frac{\partial R}{\partial D}\right\} \right) \tag{13}$$

if and only if the adjoint vector Λ satisfies the following adjoint equation.

$$\left\{\frac{\partial F}{\partial Q}\right\}^T + \Lambda^T \left[\frac{\partial R}{\partial Q}\right] = \{0\}^T \tag{14}$$

The solution vector Λ is then obtained by solving Eqn. (14) with the Euler implicit method in a time-iterative manner as

$$\left(\frac{I}{J\Delta t} + \left[\frac{\partial R}{\partial Q}\right]\right)\Delta\Lambda = -\left[\frac{\partial R}{\partial Q}\right]^T \Lambda^m - \left\{\frac{\partial F}{\partial Q}\right\}, \Lambda^{m+1} = \Lambda^m + \Delta\Lambda \tag{15}$$

where I is the identity matrix, and J represents the Jacobian matrix.

Adjoint formulation on the overset boundary can be similarly derived by slightly modifying the conventional adjoint boundary condition, which can be expressed as

$$\left[\frac{\partial R^M}{\partial Q^M}\right]^T \Lambda^M + \left[\frac{\partial R_F^S}{\partial Q^M}\right]^T \Lambda_F^S + \left\{\frac{\partial F^M}{\partial Q^M}\right\}^T = \{0\}^T \tag{16}$$

$$\left[\frac{\partial R^S}{\partial Q^S}\right]^T \Lambda^S + \left[\frac{\partial R_F^M}{\partial Q^S}\right]^T \Lambda_F^S + \left\{\frac{\partial F^M}{\partial Q^M}\right\}^T = \{0\}^T \tag{17}$$

$$\left[\frac{\partial R^M}{\partial Q_F^M}\right]^T \Lambda^M + \left[\frac{\partial R_F^M}{\partial Q_F^M}\right]^T \Lambda_F^M + \left\{\frac{\partial F^M}{\partial Q_F^M}\right\}^T = \{0\}^T \tag{18}$$

$$\left[\frac{\partial R^M}{\partial Q_F^M}\right]^T \Lambda^M + \left[\frac{\partial R_F^M}{\partial Q_F^M}\right]^T \Lambda_F^M + \left\{\frac{\partial F^M}{\partial Q_F^M}\right\}^T = \{0\}^T \tag{19}$$

where the subscript F indicates fringe cell. The superscript M and S represents the main-grid and sub-grid domain, respectively. By solving the four equations sequentially, overset boundary value on the main- and sub-grid can be updated. The update procedure of the adjoint variables on the overset boundary (Eqns. 16, 17, 18 and 19) is reverse to the conventional overset flow analysis because of the transposed operation in the adjoint formulation.

2.5 Numerical Dissipation of Adjoint Matrix

To secure stable convergence, 4th-order numerical dissipation is used for the discrete adjoint formulation[17,18]. In case that the solution from the baseline solver is evaluated using 5 stencils for 3rd order spatial accuracy which is common in conventional CFD solvers, the adjoint Jacobian matrix for 1-D problem can be represented by Eqn. (20).

$$RHS_i = -\frac{\partial R_{i+2}}{\partial Q_i}\lambda_{i+2}^m - \frac{\partial R_{i+1}}{\partial Q_i}\lambda_{i+1}^m - \frac{\partial R_i}{\partial Q_i}\lambda_i^m - \frac{\partial R_{i-1}}{\partial Q_i}\lambda_{i-1}^m - \frac{\partial R_{i-2}}{\partial Q_i}\lambda_{i-2}^m \tag{20}$$

To modify the adjoint matrix to have more diagonal dominance, a difference type symmetric equation such as numerical dissipation is needed. In the present work, 4th order numerical dissipation which is represented by the variable G is considered as shown in Eqn. (21).

$$SD_i = \varepsilon_{i+1/2}G_{i+2} - \left(3\varepsilon_{i+1/2} + \varepsilon_{i-1/2}\right)G_{i+1} + \left(3\varepsilon_{i+1/2} + 3\varepsilon_{i-1/2}\right)G_i - \left(\varepsilon_{i+1/2} + 3\varepsilon_{i-1/2}\right)G_{i-1} + \varepsilon_{i-1/2}G_{i-2} \tag{21}$$

where $0 \le \varepsilon_{i+1/2} \ll 1$ is a dissipation coefficient at the cell interface and a newly defined variable for dissipation G is

$$G_i = \frac{\partial R_i}{\partial Q_i}^T \cdot \Lambda_i \tag{22}$$

The dissipation term is added to RHS of the discrete adjoint equation as an anti-diffusion term to enhance the diagonal terms as shown in Eqn. (23).

$$\begin{aligned} RHS_i - SD_i = &-\left(\left(1+\varepsilon_{i+\frac{1}{2}}\right)\frac{\partial R_{i+2}}{\partial Q_i}^T\right)\lambda_{i+2}^m - \left(\left(1-3\varepsilon_{i+\frac{1}{2}}-\varepsilon_{i-\frac{1}{2}}\right)\frac{\partial R_{i+1}}{\partial Q_i}^T\right)\lambda_{i+1}^m - \left(\left(1+3\varepsilon_{i+\frac{1}{2}}+3\varepsilon_{i-\frac{1}{2}}\right)\frac{\partial R_i}{\partial Q_i}^T\right)\lambda_i^m \\ &-\left(\left(1-\varepsilon_{i+\frac{1}{2}}-3\varepsilon_{i-\frac{1}{2}}\right)\frac{\partial R_{i-1}}{\partial Q_i}^T\right)\lambda_{i-1}^m - \left(\left(1+\varepsilon_{i-\frac{1}{2}}\right)\frac{\partial R_{i-2}}{\partial Q_i}^T\right)\lambda_{i-2}^m \end{aligned} \tag{23}$$

The definition of the coefficient for the dissipation can be given by Eqns. (24)-(27). The proper scaling of the dissipative terms is accomplished through the factors as follow.

$$\varepsilon_{i+1/2} = \varepsilon^{(4)} C_{i+1/2}, \text{ and } C_{i+1/2} = \frac{1}{2}\left[C_{\xi_{i+1}} + C_{\xi_i} \right] \tag{24}$$

where $$C_\xi = e_\xi \varphi_\xi, \ \varphi_\xi = \sqrt{1 + (e_\eta / e_\xi)^\sigma} \ \text{ and } \ \sigma = 2/3 \ \text{(2-D case)} \tag{25}$$

And e is the spectral radius of the flux Jacobian matrices in the body-fitted curvilinear directions that conform to the body surface. A conservative estimate of this spectral radius is constructed according to the following formula,

$$e = u \cdot \hat{n} + a\sqrt{n_x^2 + n_y^2} \tag{26}$$

where a is the speed of sound at the cell center and n is the area vector at the face in the ξ -direction. The 4th order coefficient is determined by a second-order difference(smoothness) function ν.

$$\varepsilon^{(4)} = \max(0, (k^{(4)} - \varepsilon^{(2)})), \quad \varepsilon^{(2)} = k^{(2)} \max(\nu_{i,j}, \nu_{i+1,j}) \tag{27}$$

where $$\nu_{i,j} = \frac{\left| \frac{\partial C_{D_{i+1,j}}}{\partial p_{i+1,j}} - 2\frac{\partial C_{D_{i,j}}}{\partial p_{i,j}} + \frac{\partial C_{D_{i-1,j}}}{\partial p_{i-1,j}} \right|}{\left| \frac{\partial C_{D_{i+1,j}}}{\partial p_{i+1,j}} + 2\frac{\partial C_{D_{i,j}}}{\partial p_{i,j}} + \frac{\partial C_{D_{i-1,j}}}{\partial p_{i-1,j}} \right|} \tag{28}$$

and $C_{D_{i,j}}$ is the volume integrated drag coefficient on Cell (i,j). In order to prevent the deterioration of the accuracy by the dissipation term, the coefficient, $\varepsilon^{(2)}$ is taken proportional to the normalized 2nd difference of volume integrated sensitivity which acts as a sensor that turns off the dissipation around the boundary of entropy drag. As shown in Eqn. (23), the diagonal term of modified adjoint matrix becomes more dominant by considering the ratio of diagonal term to sum of off-diagonal terms and it is directly related to the stable convergence characteristics of adjoint solver.

As the dissipation increases, however, the adjoint Jacobian matrix becomes more diagonal dominance but the accuracy of the gradients decreases. Therefore, an adequate dissipation size which shows quite reasonable accuracy is taken referred from the Ref.[17] and the sensitivity analysis and design works in the present paper are performed with $k^{(4)} = 1/128$ and $k^{(2)} = 1$. However, the determination of these coefficients is still problem-dependant.

3 DESIGN OPTIMIZATION FRAMEWORK

In order to obtain high-fidelity design results, design process of a wing can be organized by multiple stages according to the goal of each design process, as shown in Figure 7. At each design stage, optimization technique is essentially determined by the number of design variable, the size of design space and the degree of non-linearity of the design space. In case of wing planform design, the range of design variables is relatively wide compared to wing surface design. Thus, a gradient-based optimization method may have some difficulties in securing a satisfactory performance even after design. This is because design space which covers a wide range of design variables may contain non-linear characteristics, and a computed solution may be trapped in local optimal region, not to mention of convergence problem. In addition, the number of design variable is at most about 4~6. Thus, global optimization method, which is time-consuming but capable of finding the optimal value in non-linear design space, can be a good choice.

On the other hand, change of design variables is much smaller in wing surface design. Thus, each design variable is not highly non-linear so that they can be approximated by 2nd order polynomial functions in a local design space, as shown in Figure 8. Moreover, surface design requires a lot of design variables which is too costly to apply global optimization techniques. In addition, most previous researches on wing surface design applied gradient-based optimization method using an adjoint method, and a shock-free wing could be successfully obtained. In the present research, we also apply adjoint approach to the 2nd stage of wing surface design.

A schematic illustration of the present design framework in a drag minimization problem is given in Figure 8. Design space is represented by a simple 3-dimensional function with respect to surface and planform design variables. From the baseline geometry at point 1, surface design process via GBOM may result in a design solution at point 2. The GBOM process including planform design variable can improve the design result from point 2 to point 3. However, the solution at point 3 may still remain as a local optimum in the given design space. If we can acquire the global optimal solution (or a better solution) through the planform design process as indicated by point 4, it is possible that the solution may reach point 5 by avoiding the local optimum between point 3 and point 5. If design space is highly non-linear in terms of surface design variables, the point 5 would still be another local optimum. Even in such case, the present design framework can provide a better alternative to cure the limitation of the GBOM approach.

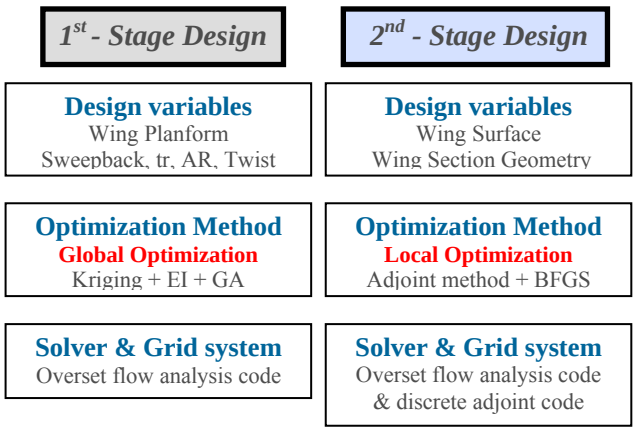

Figure 7: Strategy of 2-stage design

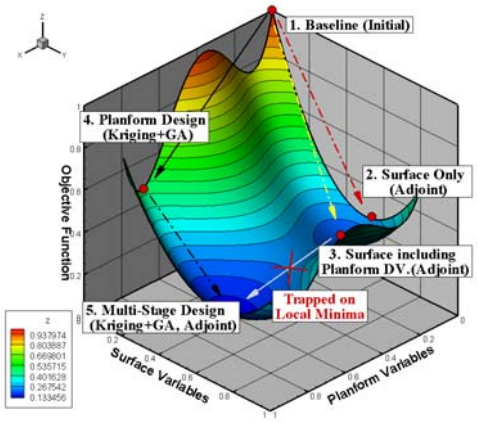

Figure 8: Schematic illustration of 2-stage design

3.1 1st –Stage Design : Planform Design using Global Optimization

As shown in Figure 9, a wing planform can be represented by several design variables such as wing span, taper ratio, sweepback angle and twist angle. GA optimizer can be directly used for finding the global optimum values at the expense of huge computational cost. Generally, GA needs thousands times of flow analyses for only a few design variables. For efficient global optimization, a meta-model is firstly constructed using Kriging model, and then GA is introduced to find the global optimal geometry from the meta-model. Experimental data points are determined through Central-Composite Experimental Design (CCD) method based on Design of Experiment (DOE) theory, and the solution at each experimental point are evaluated by CFD solver. Using the evaluated experimental points, the meta-model can be constructed. After that, GA optimizer is applied to find the optimal geometry with respect to wing planform design variables. However, this approach might have a possibility to miss the global

optimum, especially experimental data points are not good enough. Thus, additional data points based on the searching algorithm of EI are added. As a preliminary case of the present multi-stage design approach, ONERA-M6 wing is considered. Planform design variables are shown in Figure 9 and Table 1. As shown in Eqn. (29), the objective of design process is to minimize drag coefficient, while lift coefficient is maintained as the value of the baseline model. In order to provide physically meaningful design results, a wing weight constraint obtained by statistical group weight method[23] is incorporated. The optimizer tends to increase the span to reduce induced drag, and decrease the thickness of wing section to reduce wave drag. Without the constraint of the wing weight, the designed wing could be unrealistic in terms of structural safety and fuel storage. Wing weight during the design process is imposed not to exceed the baseline wing weight.

$$\begin{aligned} &Minimize : C_D \\ &Subject\ to : C_L \geq C_{L_0}, C_{L_0} = (Lift\ coefficient\ of\ Baseline\ Model) \\ &W_{W_0} \geq W_W, W_{W_0} = (Wing\ weight\ of\ Baseline\ Model) \end{aligned} \tag{29}$$

The free stream Mach number is 0.84, and the angle of attack is 3.06 degree. The governing equations are the three-dimensional compressible Euler equations. For the spatial discretization, RoeM scheme[24] is used, and MUSCL(Monotonic Upstream Centered Scheme for Conservation Law) approach using a third order interpolation is applied for a higher order spatial accuracy. For time integration, LU-SGS scheme is applied.

Design variable(Dv)		Min	Baseline	Max	Kriging1	Kriging2	Kriging-EI
Dv1	Sweepback Angle (Λ)	25°	30	35°	34.998	None	33.6972°
Dv2	Half Span $(b/2)$	1.3240	1.4712	1.6183	1.536752	None	1.466160
Dv3	Taper Ratio (c_2/c_1)	0.5058	0.562	0.6182	0.549260	None	0.527694
Dv4	Twist Angle (θ)	-2°	0	2°	-0.000058	None	-0.01867°

Table 1: Geometric information of ONERA-M6 and the designed wing

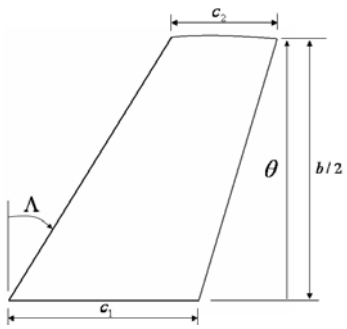

Figure 9: Planform variables of ONERA-M6

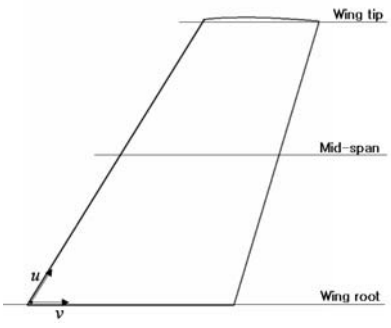

Figure 10: Surface variables of ONERA-M6

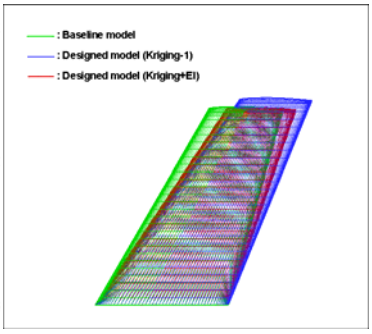

Figure 11: Comparison of baseline model with designed model

Table 1 shows a set of planform variables, and Table 2 is the comparison of predicted values and real values for the optimal geometry. Predicted values show a pretty good agreement with real values, which indicates that the planform design tool works well. Kriging-1 is the case obtained without weight constraint, while weight constraint is included in Kriging2 and Kriging-EI. The predicted values of sweepback angle and half span in Kriging1 are substantially larger than the baseline geometry which may cause structural problem. On the other hand, the Kriging-2 fails to predict an

optimum point within constrained boundaries. This is caused by the insufficient number of sample points. For that reason, additional sample point by EI, which is expected to improve the objective function value, is iteratively added until any additional EI point is not obtained. As shown in Table 2, when just comparing the objective values, Kriging-1 appears to be better than Kriging-EI but it does not consider the wing weight. Hence, Kriging-EI produces a more realistic design solution.

Obj. fn. & Constraint	Baseline model	Kriging1 + GA		Kriging2 + GA		Kriging-EI + GA	
		Predicted	Real value	Predicted	Real value	Predicted	Real value
C_L	0.261746	0.26174	0.2601053	None	None	0.260879	0.2602198
C_D	0.011937	0.01059	0.0103969	None	None	0.010961	0.0111651
Weight	6.497615	Not included (7.208778)		None		6.4926028	

Table 2: Comparison of objective function and constraint values (planform design/ONERA-M6)

Figure 11 depicts the baseline and designed planforms from Kriging model. Figure 13 and 14 show pressure contours of the designed model. The pressure contour shows that shock strength is weakened after design, and as mentioned before, Kriging1 is better than Kriging-EI. However, shock waves on upper wing surface are not remarkably weakened in both results. It is because drag reduction during the planform design comes from both the reduction of induced drag and wave drag. Thus, as shown in Table.4, drag decomposition method needs to be introduced to identify the portion of induced drag reduction from the whole drag reduction. Detailed analysis will be given in section 3.2.

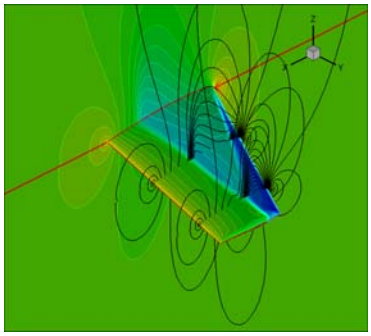

Figure 12: Pressure contour of baseline model

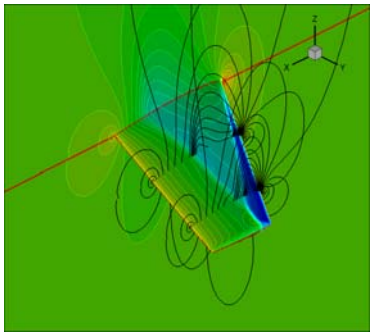

Figure 13: Pressure contour of designed planform by kriging1 method

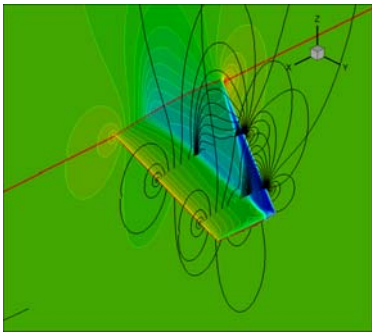

Figure 14: Pressure contour of designed planform by kriging-EI method

3.2 2nd-Stage Design : Surface Design Using Local Optimization

With the planform geometry obtained at 1st stage design, surface design is directly performed by discrete adjoint approach. Since a large number of design variables are usually required to control change of wing surface geometry, adjoint approach is much more appropriate. As shown in Figure 10, three design sections are defined along the span-wise direction. 10 design variables are positioned at each design section of upper and lower surface, respectively. Total 60 design variables are used in this case. Wing surface at each section is deformed by using the Hicks-Henne functions. Design formulation is given by Eqn. (30). In order to calibrate the variation of drag and lift coefficients, the weight factor for the lift constraint is given by the sensitivity ratio of drag to lift coefficient with respect to the angle of attack.

$$\begin{gathered} Minimize: C_D \\ Subject\ to: C_L \geq C_{L_0}, C_{L_0} = (Lift\ coefficient\ of\ Baseline\ Model) \\ (Objective\ function) = C_D + Wt \times \left[0, C_{L_0} - C_L\right], \quad Wt = \frac{\partial C_D}{\partial \alpha} \Big/ \frac{\partial C_L}{\partial \alpha} \end{gathered} \tag{30}$$

After 2-stage design, lift coefficient slightly decreases(0.6% reduction) but drag coefficient decreases from 0.011937 to 0.0075882(36.4% reduction). Consequently, *L/D* is enhanced from 21.927 to 34.227(56.3% increase) as shown Figure 16, and the Λ shock on the upper wing surface is remarkably weakened as shown in Figure 15.

Obj. fn. & Constraint	Baseline model	Planform design only	Surface design only (Adjoint)	Multi-stage design
		Kriging-EI + GA		Kriging-EI + GA + Adjoint
C_L	0.261746	0.2602198	0.259997	0.2601049
C_D	0.011937	0.0111651	0.007868	0.0075882

Table 3: Comparison of objective function/costraint values for designed model (ONERA-M6)

Drag coefficient is decomposed by using wake integration method (far-field method) to investigate the behavior of each drag component after wing planform and surface optimization, as shown in Table 4. In viscous flow, shock strength is relatively weak due to viscous effect. On the other hand, flow over wing upper surface is more accelerated in inviscid analysis, which induces a strong shock. Thus, the portion of induced drag is not so large compared with entropy drag. It can be seen that entropy drag reduction at each design stage is larger than induced drag reduction, and entropy drag substantially decreases after surface design.

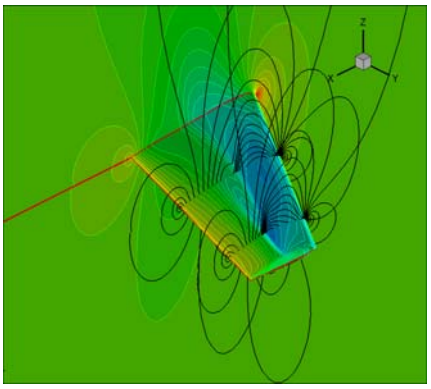

Figure 15: Presssure contour of 2-stage designed model

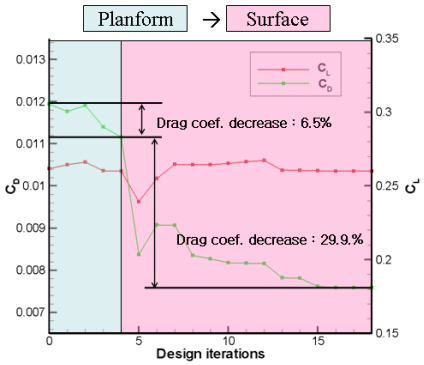

Figure 16: 2-stage design history of ONERA-M6 (inviscid design)

Design strategy	Drag prediction method	C_L	C_D	C_D - entropy	C_D - induced
Baseline model	Surface integration	0.261746	0.011937	N/A	N/A
	Wake integration	0.267401	0.010837	0.00738432	0.00345286
Planform only (Kriging-EI + GA)	Surface integration	0.260219	0.011165	N/A	N/A
	Wake integration	0.270864	0.009873	0.00630170	0.00357173
Surface only (AV + BFGS)	Surface integration	0.259997	0.007868	N/A	N/A
	Wake integration	0.270641	0.007347	0.00360265	0.00374472
2-stage design	Surface integration	0.260104	0.007588	N/A	N/A
	Wake integration	0.262512	0.007124	0.00362269	0.00350174

Table 4: Comparison of aerodynamic performances evaluated by drag decomposition method

4 MULTI-STAGE DESIGN APPLICATIONS

The final goal of the present work is development of high fidelity and efficiency aerodynamic optimization tool which can be applied to practical applications such as complex geometry. Therefore, the 7 block overset mesh system of DLR-F4 wing-body configuration, the test geometry in the 1st Drag Prediction Workshop (DPW-I), is considered. At the first design case, the transonic wing (ONERA-M6) with overset mesh system is re-designed in viscous flow condition. After that, inviscid and viscous designs of DLR-F4 geometry are carried out sequentially following the 2-stage design process.

4.1 Viscous Design of Transonic Wing

The first design problem is re-design of transonic wing with relatively simple 2 block overset mesh system. The flow condition and definition of design problem are same as test design case except the viscous flow condition. Reynold number 14.6 million and 3-dimensional overset Navier-Stokes solver with $k-wSST$ turbulence model is applied. To determine the sample experimental data points, Latin Hypercube Sampling(LHS) based on space filling method is applied and 41sample points are supplied as initial experimental points.

Design variable(Dv)		Min	Baseline	Max	Kriging-EI(inviscid)	Kriging-EI(viscous)
Dv1	Sweepback Angle (Λ)	25°	30	35°	33.6972°	32.9786°
Dv2	Half Span $(b/2)$	1.3240	1.4712	1.6183	1.466160	1.43395
Dv3	Taper Ratio (c_2/c_1)	0.5058	0.562	0.6182	0.527694	0.54987
Dv4	Twist Angle (θ)	-2°	0	2°	-0.01867°	-0.031334°

Table 5: Geometric parameters of transonic wing and designed wing

Obj.-Fn. & constraint	Baseline model	1st –stage design	2nd –stage design
		Planform design	Surface design
C_L	0.2618	0.25962	0.26182
C_D	0.01751	0.01691	0.01446
Weight	6.52404	6.49503	N/A

Table 6: Comparison of objective function & constraint values

Table 5 and 6 are the 2-stage viscous design result of transonic wing. The modification of planform design variables shows similar trend to the inviscid design result. The drag coefficient decreases from 0.01751 to 0.01446(17.3% reduction) while lift coefficient decreases 0.1% after 2-stage design and *L/D* is enhanced from 14.97 to 18.10. The amount of drag reduction is about half of the inviscid case due to the viscous drag and Table 7 shows the each drag component. However, when comparing entropy drag component with the inviscid case(Table 4) which comes from shock wave only, shock wave in viscous design case is weaken more than inviscid case. Figure 20 shows more clearly that the Λ shock on the upper wing surface is almost disappeared.

Design strategy	Dreg prediction	C_L	C_D	C_D -entropy	C_D -induced
Baseline model	Surface integration	0.262187	0.017506	N/A	N/A
	Wake integration	0.292724	0.016039	0.0128468	0.0031921
Planform only (Kriging-EI+GA)	Surface integration	0.259623	0.016913	N/A	N/A
	Wake integration	0.288164	0.015516	0.0119126	0.0036035
2-stage design	Surface integration	0.261824	0.014463	N/A	N/A
	Wake integration	0.297502	0.011227	0.0072514	0.0039755

Table 7: Comparison of aerodynamic performances evaluated by drag decomposition method

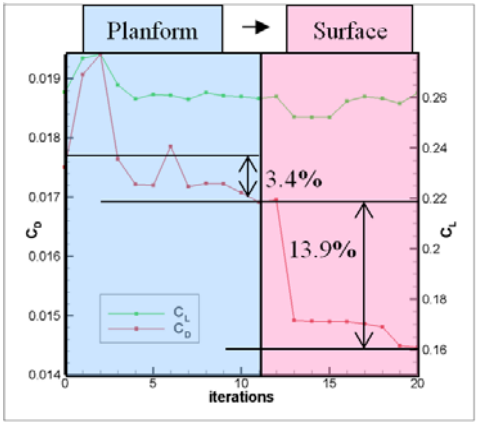

Figure 17: 2-stage design history of ONERA-M6

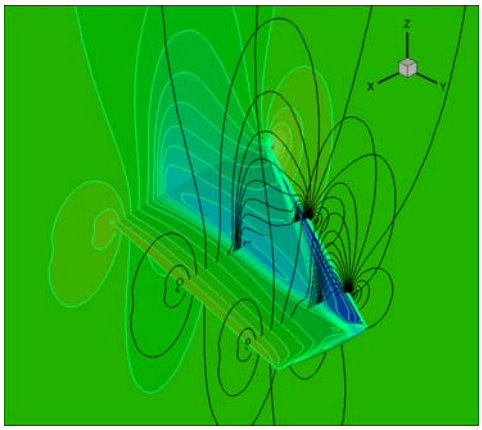

Figure 18: Pressure contour of baseline model

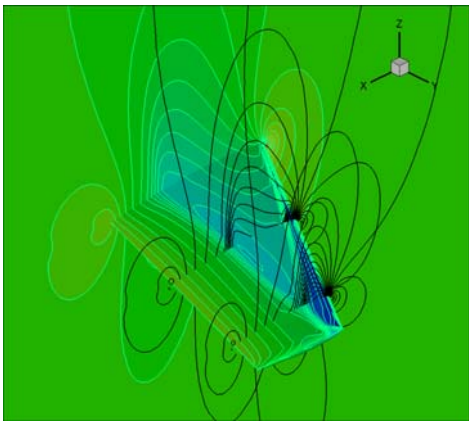

Figure 19: Pressure contour of 1st-stage designed model

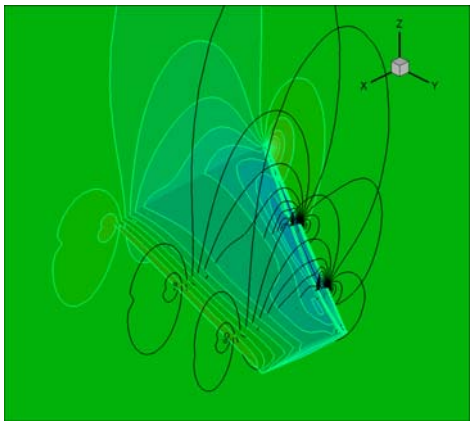

Figure 20: Pressure contour of 2nd-stage designed model

4.2 Inviscid Design of DLR-F4

As a second design case, shape optimization of DLR-F4 wing-body geometry is carried out in inviscid flow condition. Figure 21 and 22 shows design variables. Variables for planform design are span, chord length at the kink and wing tip position, sweep-back angle and twist angle. Surface design sections are defined along the span-wise direction by considering large aspect ratio of the baseline wing. 10 design variables are positioned at each section of upper and lower surface, respectively. Total 200 design variables are used. Wing surface at each section is deformed using the Hicks-Henne functions. Regions between design sections are deformed by using linear interpolation.

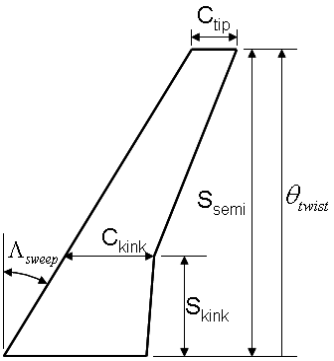

Figure 21: Wing planform design variables of DLR-F4

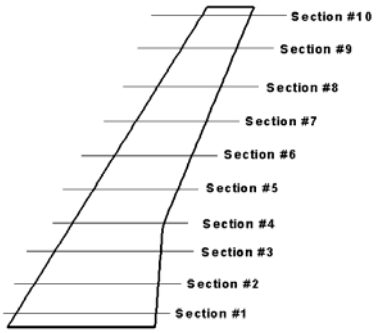

Figure 22: Surface variables of DLR-F4

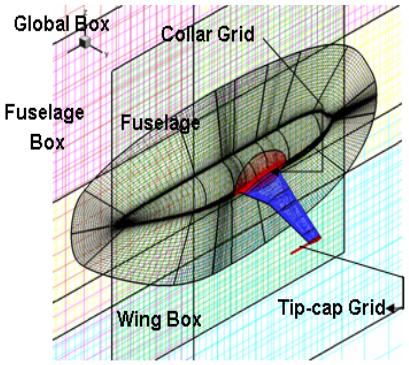

Figure 23: Overset grid system for DLR-F4

In order to compute multi-body configuration, overset mesh system is used. Figure 23 shows the overall mesh system composed of 7 blocks: a global box, a fuselage box, a wing box, a fuselage block (O-O type), a collar block (O-H type), a wing block (O-H type), and a tipcap block (C-type). The total number of mesh point is about 1.22 million. The collar block is positioned at the interface of wing and fuselage, and a tipcap block on the wing tip to maintain a high-quality mesh. The free stream Mach number is 0.75, the angle of attack is zero. Numerical techniques for flow analysis and are the same as the inviscid design case of the ONERA-M6 wing. Objective functions and constraint for 2-stage design are also same with the first design case.

Table 8 presents the comparison of the baseline and the designed geometries using Kriging model and Kriging-EI method. As shown in Table 8 and Figure 24, the change of design variables is relatively small because of weight constraint. This tendency is also shown in ONEAR-M6 wing design problem which uses weight constraint, and it demonstrates that the statistical group weight method using in this study adequately works as a constraint. Table 9 shows 2-stage design results and both Kriging and Kriging-EI methods improve aerodynamic performance even though the change of design variables is relatively small.

Design variable(Dv)		Min	Baseline	Max	Opt. Kriging	Opt. Kriging-EI
Dv1	Sweepback Angle (Λ)	25°	27.15°	30°	27.187492	27.03516°
Dv2	Kink-Span(S_{kink})	3733.5	4148.6	4563.2	3886.7324	3908.1826
Dv3	Semi-Span(S_{semi})	11682.0	12980.5	14273.0	12840.069	12990.120
Dv4	Kink-Chord(C_{kink})	2731.2	3034.7	3338.1	3138.7873	3160.5550
Dv5	Tip-Chord(C_{semi})	1401.0	1556.7	1712.4	1570.0544	1501.5888
Dv6	Twist Angle (θ)	-5.0°	-4.631°	-3.0°	-4.445511°	-4.603918°
Const.	Wing Weight(W_{W_0})		14.3024		14.284285	14.299511

Table 8: Design variables and optimum values of DLR-F4 wing/body

Obj. fn. & Constraint	Baseline model	1st-stage design		2nd-stage design
		Kriging + GA	Kriging-EI + GA	Kriging-EI + Adjoint
C_L	0.710176	0.708225	0.711111	0.7077625
C_D	0.023014	0.021064	0.020632	0.0202102

Table 9: Comparison of objective function and constraint values (2-stage design/DLR-F4)

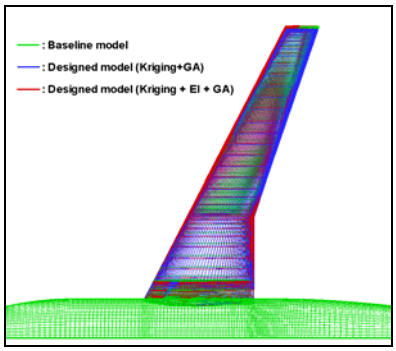

Figure 24: Comparison of baseline model with designed models (kriging method)

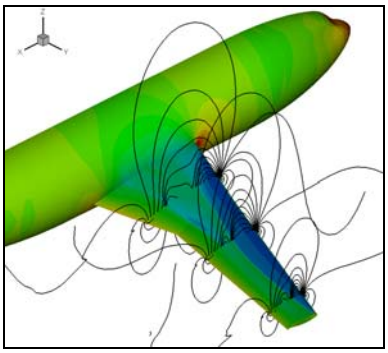

Figure 25: Pressure contour of baseline model

After 2-stage design process, drag coefficient decreases by 12.3%, and variation of lift coefficient during the design process is less than 0.3% of the initial value as shown Figure 26. As the result, *L/D* increases from 30.85 to 35.02 after the 2-stage design process. It is observed that shock strength on wing surface from root and mid-span is almost eliminated after the 2-stage design process as shown in Figure 28, and shock wave on the wing tip is weakened though it does not decrease as much as mid-span.

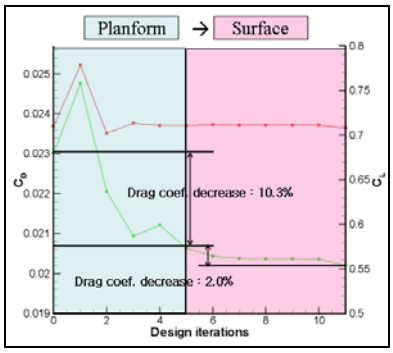

Figure 26: 2-stage design history of DLR-F4

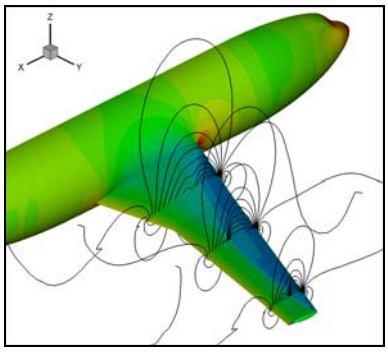

Figure 27: Pressure contour of 2-stage designed model

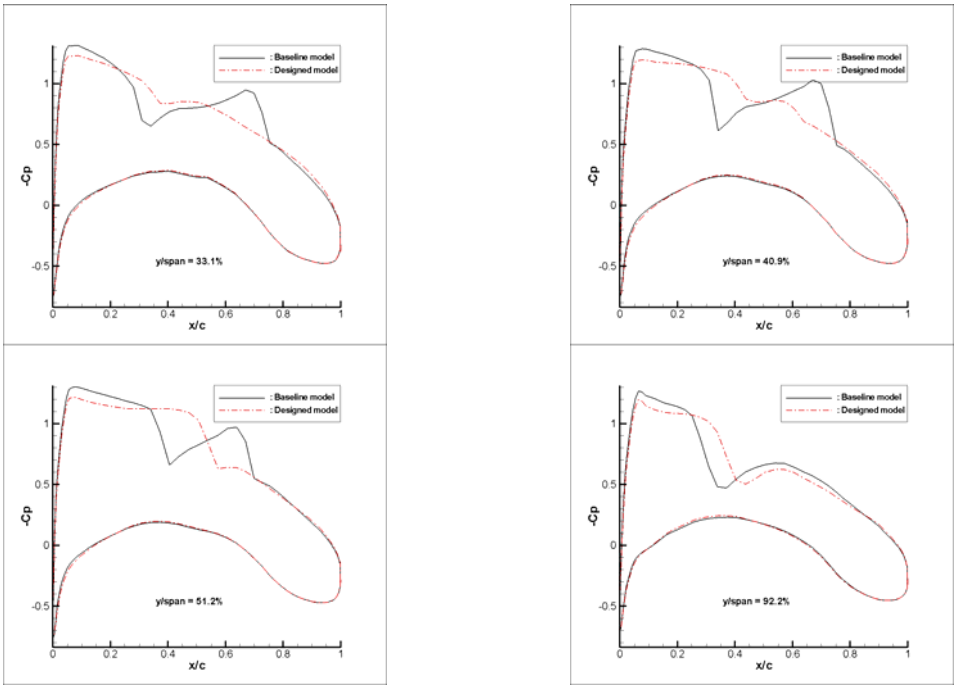

Figure 28: Surface pressure distribution

4.3 Viscous Design of DLR-F4

For the final practical design case, viscous design of DLR-F4 is performed. To secure the accuracy of flow solution at boundary layer, sub-cell TFI(Transfinite Interpolation) is applied where the surfaces are overlapped at the block interface such as fuselage-collar, collar-wing and wing-tipcap interface. The free stream Mach number is 0.75, the angle of attack is 0.0 degree and Reynolds number is 3×10^6, which corresponds to the cruising condition. 7 blocks overset grid system which has same grid topology with inviscid design is used and the total number of mesh point is 3.2million.

Design variable(Dv)		Min	Baseline	Max	Kriging-EI(inviscid)	Kriging-EI(viscous)
Dv1	Sweepback Angle (Λ)	25°	27.15°	30°	27.03516°	25.24544°
Dv2	Kink-Span(S_{kink})	3733.5	4148.6	4563.2	3908.1826	4322.3576
Dv3	Semi-Span(S_{semi})	11682.0	12980.5	14273.0	12990.120	12875.270
Dv4	Kink-Chord(C_{kink})	2731.2	3034.7	3338.1	3160.5550	3252.0836
Dv5	Tip-Chord(C_{semi})	1401.0	1556.7	1712.4	1501.5888	1709.6295
Dv6	Twist Angle (θ)	-5.0°	-4.631°	-3.0°	-4.603918°	-4.9590°
Const.	Wing Weight(W_{W_0})		14.3024		14.299511	14.29989

Table 10: Design variables and optimum values of DLR-F4 wing/body

Obj.-Fn. & constraint	Baseline model	1st –stage design	2nd –stage design
		Planform design	Surface design
C_L	0.491270	0.491078	TBA
C_D	0.032227	0.031038	TBA
Weight	14.3024	14.29989	N/A

Table 11: Comparison of objective function & constraint values

Table 10 shows the 1st-stage design result. The modification of planform variables is slightly different from inviscid case while the transonic wing case which shows similar modification trend. It may be caused by geometry distinction between transonic wing and wing-body. Moreover, additional 2 kink parameter for planform variable makes DOF of design space higher than the simple transonic wing case. Reduction of Drag coefficient may look like that the improvement of the present design is less impressive compared to inviscid case. However, the drag, which is caused by the fuselage, remains at a constant value through the whole design process, because design variables are applied to the wing section only. Thus, the portion of fuselage drag actually increases as the whole drag coefficient decreases at each design step. If effects of the fuselage are considered in actual design process, aerodynamic performance could be more improved than the present result.

After the planform design, surface design process is still running. The author regrets that fully converged 2-stage design results are not included in this paper because viscous wing-body design requires more computational cost than what we expected. The final results will be shown in the presentation.

5 CONCLUSION

An efficient high-fidelity multi-stage design optimization approach is proposed by combining global and local optimization techniques. At 1st stage design, wing planform design is carried out by GA optimizer based on the Kriging method. Additional sample points using the EI algorithm are efficiently added into Kriging model for the enhanced global search of wing planform geometry. At 2nd stage design, wing surface is then modified by the GBOM approach based on the discrete adjoint method which brings a substantial reduction of wave drag. To secure stable convergence characteristics of adjoint solver, a 4th-order numerical dissipation is used for the discrete adjoint formulation. Performance improvements of the designed model are evaluated through the drag decomposition technique. The portion of induced drag and wave drag analyzed by drag decomposition can provide concrete information on dominant design parameter and/or stage for drag reduction. The proposed design approach is applied to the re-design of the ONERA-M6 wing and DLR-F4 wing/body configuration using overset inviscid and viscous flow analysis/adjoint codes. Results of the two design cases demonstrate that the proposed multi-stage design approach can efficiently improve the aerodynamic performance of three-dimensional aircraft configuration by exploiting advantages of the global and local optimization methods. Especially, the proposed multi-stage design approach is expected to be quite useful to deal with design problems with drastic geometric change where gradient-based optimization methods might have some difficulties.

ACKNOWLEDGEMENT

This work is supported by the Korea Science and Engineering Foundation (KOSEF) grant funded by the Korea government (MEST) (No.20090084669), NSL (National Space Lab.) program through the National Research Foundation of Korea funded by the Ministry of Education, Science and Technology (Grant 20090091724). The authors also would like to acknowledge the financial support from Agency for Defense Development, the second stage of the Brain Korea-21 Project for the Mechanical and Aerospace Engineering Research at Seoul National University.

REFERENCES

[1] John McCall, Genetic algorithm for modelling and optimization, *Journal of Computational and Mathematics*, Vol. 184, 2005.

[2] H.S Chung and J.J Alonso, Multi-objective Optimization using Approximation Model-Based Genetic Algorithm, 10th AIAA/ISSMO, *Multidisciplinary Analysis and Optimization Conference*, AIAA 2004-4325 Albany, NY, September 2004.

[3] Wataru YAMAZAKI, Kisa MATSUSHIMA and Kazuhiro NAKAHASHI, Aerodynamic Shape Optimization Based on Drag Decomposition, *24th Applied Aerodynamics Conference*, AIAA-2006-3332, 2006.

[4] R.H. Myers, and D.C. Montgomery, Response surface methodology: process and product optimization using design experiments, Wiley, New York, 1978.

[5] Ahn.J.K., Kim.H.J., Lee.D.H. and Rho.O.H., Response Surface Method for Aircraft Design in Transonic Flow, *Journal of Aircraft*, Vol. 38, No.2, pp.231-238.2001.

[6] Jerome Sacks, William J. Welch, Toby J. Mitchell and Henry P. Wynn, Design and Analysis of Computer Experiments, *Statistical Science*, Vol. 4, No. 4, pp. 409-435, 1989.

[7] Timothy W. Simpson, Timothy M. Mauery, John J. Korte and Farrokh Mistree, Comparison of response surface and kriging models for multidisciplinary design optimization, *American Institute of Aeronautics and Astronautics*, AIAA-98-4755, 1998.

[8] Donald R. Jones, Matthias Schonlau and William J. Welch, Efficient Global Optimization of Expensive Black-Box Function, *Journal of Global Optimization*, Vol. 13, pp.455-492, 1998.

[9] Mockus J., Tiesis V. and Zilinskas A., The Application of Bayesian Methods for Seeking the Extremum, *Toward Global Optimization*, Vol. 2, pp.117-129, 1978.

[10] Shinkyu Jeong, Mitsuhiro Murayama and Kazuomi Yamamoto, Efficient Optimization Design Method Using Kriging Model, *Journal of Aircraft*, Vol. 42, No.2, pp.413-420, 2005.

[11] Kasidit Leoviriyakit and Antony Jameson, Multi-point Wing Planform Optimization via Control Theory, *43rd Aerospace Science Meeting and Exhibit*, 2005-0450, January 10-13,Reno, Nevada, 2005.

[12] B. J. Lee and C. Kim, Automatic Design Methodology of Turbulent Internal Flow using Discrete Adjoint Formulation, *Journal of Aerospace Science and Technology*, Vol.11, 2007, pp. 163,173.

[13] B. J. Lee and C. Kim, Aerodynamic Redesign Using Discrete Adjoint Approach on Overset Mesh System, *Journal of Aircraft*, Vol.45. No.5. 2008, pp.1643, 1653.

[14] Dimitri J. Marvrisplis, Discrete Adjoint-Based Approach for Optimization Problems on Three-Dimensional Unstructured Meshes, *AIAA Journal*, Vol. 45, No. 4, April, 2007.

[15] E.J Nielsen and W.K Anderson, Recent Improvements in Aerodynamic Design Optimization on Unstructured Meshes, *AIAA Journal*, Vol. 40, No. 6, pp. 1155-1163, 2002.

[16] S. Koc, H. Kim and K. Nakahashi, Aerodynamic Design Optimization of Wing-Body Configuration, *AIAA paper*, 2005-331.

[17] B. J. Lee and Chongam Kim, Strategies for Robust Convergence Characteristics of Discrete Adjoint Solver, *5th International Conference of Computational Fluid Dynamics*, 2008.

[18] Byung Joon Lee, Meng-Sing Liou and Chongam Kim, Optimizing a Boundary-Layer-Ingestion Offset Inlet by Discrete Adjoint Approach, *AIAA Journal*.(Accepted)

[19] R.M. Cumming, M.B. Giles and G.N. Shrinivas, Analysis of the Elements of Drag in Three-Dimensional Viscous and Invicid Flow, *AIAA paper* 96-2482-CP, 1996.

[20] Micheal B. Giles and Russell M. Cummings, Wake Integration for Three-Dimensional Flowfield Computation: Theoretical Development, *Journal of Aircraft*, Vol. 36, No. 2, pp.357-365. 1999.

[21] C.P. van Dam, Recent experience with different methods of drag prediction, *Progress in Aerospace Science* 35 (1999), pp. 751-798. 1996.

[22] Luigi Paparone and Renato Tognaccini, Computational Fluid Dynamics-Based Drag Prediction and Decomposition, *Journal of Aircraft*, Vol. 41, No. 9, pp.1647-1657. 2003.

[23] Kasidit Leoviriyakit and Antony Jameson, Aerodynamic Shape Optimization of Wings including Planform Variations, *41th AIAA Aerospace Science Meeting and Exhibit*, 2003-0210, January 6-9, Reno, Nevada, 2003.

[24] Sung-soo Kim, Chongam Kim, Oh-hyun Rho, and Seung Kyu Hong, Cures for the Shock Instability: Development of Shock-Stable Roe Scheme, *Journal of Computational Physics*, Vol. 182, No. 2, 2003, pp. 342-374.